Forced and Internal Twentieth-Century SST Trends in the North Atlantic*

MINGFANG TING, YOCHANAN KUSHNIR, RICHARD SEAGER, AND CUIHUA LI

Lamont-Doherty Earth Observatory, Columbia University, Palisades, New York

(Manuscript received 7 April 2008, in final form 26 September 2008)

ABSTRACT

In recent years, two alarming trends in North Atlantic climate have been noted: an increase in the intensity and frequency of Atlantic hurricanes and a rapid decrease in Greenland ice sheet volume. Both of these phenomena occurred while a significant warming took place in North Atlantic sea surface temperatures (SSTs), thus sparking a debate on whether the warming is a consequence of natural climate variations, anthropogenic forcing, or both; and if both, what their relative roles are. Here models and observations are used to detect and attribute long-term (multidecadal) twentieth-century North Atlantic (NA) SST changes to their anthropogenic and natural causes. A suite of Intergovernmental Panel on Climate Change (IPCC) twentieth-century (C20C) coupled model simulations with multiple ensemble members and a signal-to-noise maximizing empirical orthogonal function analysis are used to identify a model-based estimate of the forced, anthropogenic component in NA SST variability. Comparing the results to observations, it is argued that the long-term, observed, North Atlantic basin-averaged SSTs combine a forced global warming trend with a distinct, local multidecadal ''oscillation'' that is outside of the range of the model-simulated, forced component and most likely arose from internal variability. This internal variability produced a cold interval between 1900 and 1930, followed by 30 yr of relative warmth and another cold phase from 1960 to 1990, and a warming since then. This natural variation, referred to previously as the Atlantic Multidecadal Oscillation (AMO), thus played a significant role in the twentieth-century NA SST variability and should be considered in future, near-term climate projections as a mechanism that, depending on its behavior, can act either constructively or destructively with the region's response to anthropogenic influence, temporarily amplifying or mitigating regional climate change.

1. Introduction

The extremely active and destructive hurricane season in 2005 sparked an intense debate as to whether or not the intensification of hurricane activity during recent decades was due to natural variability or anthropogenic forcing. At the center of the debate is the cause and impact of the concomitant warming over the North Atlantic (NA). A few recent studies (e.g., Emanuel 2005; Webster et al. 2005; Santer et al. 2006) linked the increase in the intensity of the Atlantic hurricanes to the rise in tropical Atlantic SST and suggested that the latter is due to global warming. Other studies argued that naturally occurring multidecadal SST variability is the main source of the recent increases in Atlantic hurricane activity (Goldenberg et al. 2001; Landsea 2005).

The recent warming trend in tropical North Atlantic sea surface temperature (SST) is consistent with a coherent, North Atlantic basinwide SST warming, as can be clearly seen in the North Atlantic basin average and annual mean SST anomaly index (NASSTI) shown in Fig. 1.[1] The solid black line in this figure displays an overall gradual warming culminating in a rapid upward trend from 1975 to the present. The trend is obviously not linear and includes an ''oscillatory'' component with a relatively cold episode from 1900 to 1925, followed by

* Lamont-Doherty Earth Observatory Contribution Number 7204.

Corresponding author address: Mingfang Ting, Lamont-Doherty Earth Observatory, 61 Rt. 9W, Columbia University, Palisades, NY 10964.
E-mail: ting@ldeo.columbia.edu

[1] The annual mean NA SST anomaly in Fig. 1 is defined as deviations of the basinwide average SST from its long-term mean for the entire twentieth century. It was also subjected to a recursive Butterworth filter with a half power point at a period of 10 yr, so that variability with time scales shorter than 10 yr has been strongly reduced.

DOI: 10.1175/2008JCLI2561.1

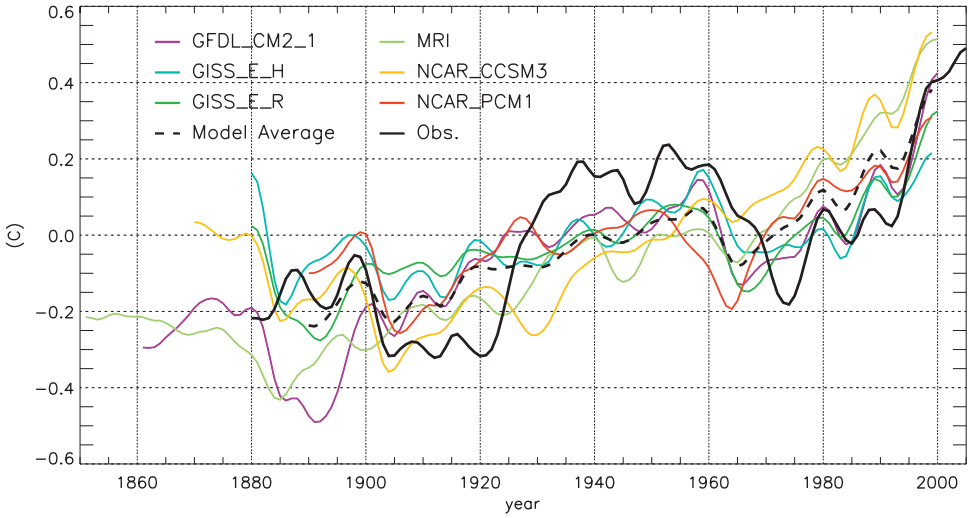

FIG. 1. NASSTI averaged over the ocean grids from the equator to 60°N and from 7.5° to 75°W. Black solid line: observations; color lines: coupled ocean–atmosphere models of the IPCC twentieth-century simulations averaged over multiple realizations starting from different initial conditions; dashed black line: average of all models. The index is defined as the deviation from long-term climatological mean for the entire twentieth century and the time series are subject to a low-pass tangent Butterworth filter with a 10-yr cutoff.

a warmer period from 1930 to 1960, another relatively cold period from 1970 to 1990, and finally the recent rapid warming, all superimposed on the general rise of temperatures. The combination of an upward trend plus a multidecadal oscillatory component indicates the possible superposition of an externally forced component and an internally generated one. The latter is consistent with the North Atlantic multidecadal SST variation that was identified in several previous studies (e.g., Kushnir 1994; Schlesinger and Ramankutty 1994; Enfield et al. 2001) and is commonly referred to as the Atlantic Multidecadal Oscillation (AMO) after Kerr (2000).

The characteristics of the observed NASSTI trend in Fig. 1 raise several questions. First, is it possible to confirm that the observed temporal dependence results from the superposition of significant internal variability (AMO) on the response to external forcing? If so, what is the best way to quantify the two components in observations? Second, what is the climatic impact of each component in different regions of the world? Answers to these questions are important for designing a useful ''near term'' climate prediction system to help plan and prepare for climate change in the coming few decades.

Figure 2 shows the application of two of the previously proposed approaches designed to remove the forced signal associated with both anthropogenic and other natural (volcanic and solar) forcing from the total observed NASSTI, with the purpose of uncovering the internal component of the variability. The first commonly used method is to remove the linear trend from the observed North Atlantic SST index, as shown in Fig. 2a (e.g., Enfield et al. 2001; Sutton and Hodson 2005; Knight et al. 2006). This method assumes that the forced trend is linear and uniform over time. The linear detrending method suggests that the positive anomaly in NASSTI at the end of the twentieth century (0.4°C) is equally divided between the externally forced trend and the internal AMO variability (amplitude 0.2°C) and that the latter is currently at a peak state, similar to its state in the middle of the twentieth century. A second method is to use the global mean sea surface temperature as a proxy for the externally forced signal (Trenberth and Shea 2006; Mann and Emanuel 2006). When subtracting the global mean SST anomalies from the tropical North Atlantic SST to remove the forced signal, Trenberth and Shea (2006) concluded a predominant contribution from the anthropogenically forced warming to the total North Atlantic SST anomalies. In this study, we regress the two-dimensional SST field on the time series of globally averaged SST (SSTg) and obtain an estimate of the internal component as the local difference between the total field and the regression pattern. The North Atlantic average of both the regressed NASSTI and the residual is shown in Fig. 2b. The regression method used here accounts for the fact that the forced SST is not uniform spatially, which differs from that used in Trenberth and Shea (2006).

Comparing Figs. 2a and 2b, one sees that the two methods imply considerable differences in the amplitude and temporal properties of the forced and internal

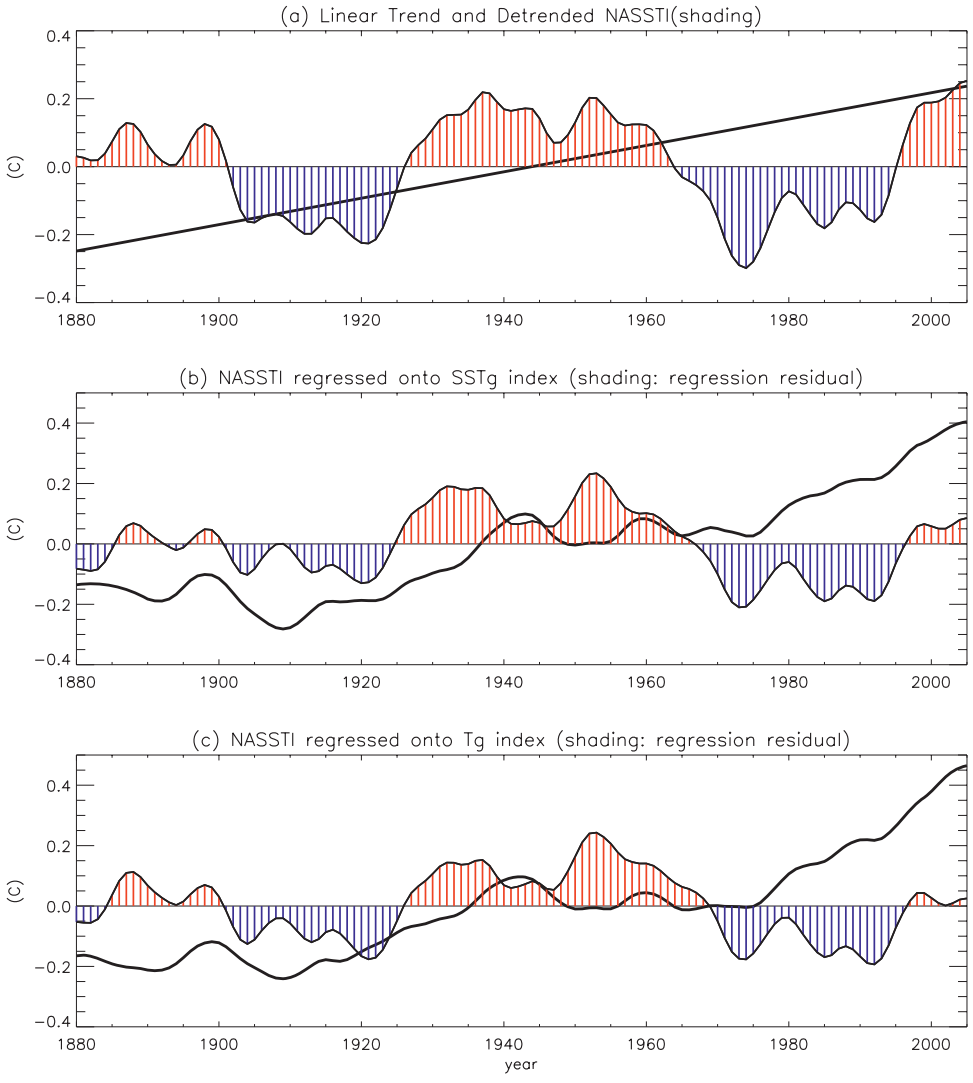

FIG. 2. (a) The linear trend (solid black line) and detrended NASSTI (shaded). (b) NASSTI regressed onto the global mean SST (SSTg regression, solid black line) and the difference between the observed NASSTI shown in Fig. 1 and the SSTg regression (shaded). (c) NASSTI regressed onto the global mean surface temperature (Tg regression, solid black line) and the difference between the observed NASSTI shown in Fig. 1 and the Tg regression (shaded).

variability. Unlike linear detrending, regression on the global mean SST implies that the positive NASSTI anomaly at the end of the twentieth century is largely due to the forced signal (~0.34°C) and only a small portion is caused by internal AMO variability (~0.06°C), consistent with Trenberth and Shea (2006). Furthermore, although linear detrending might suggest that the AMO is at its peak amplitude and that the internal variability in the next 2 decades would stay at the same amplitude or decrease, regression on the global mean SST suggests that the internal component of the AMO could cause even warmer north Atlantic SST in the coming years. Another commonly used measure of the anthropogenically forced variability is the global mean surface temperature (Tg), as shown in Fig. 2c. This method suggests an even weaker recent warming due to internal variability than when global mean SST is used, leaving the externally forced signal to explain almost all of the observed change during the late twentieth century. In addition to the difference in relative contribution to forced and internal components of NASSTI, the overall amplitude of the AMO is about 20% weaker using the global mean SST and global mean surface temperature as a proxy for forced trend. Given these differences, it is important to find an objective, quantitative way to measure the realism of each method. We attempt this by making

use of both observations and model estimates of externally forced climate change.

2. Ratio of forced and internal variability in coupled models

In this study, we separate the forced and internal components of the North Atlantic decadal SST variability by using all the Intergovernmental Panel on Climate Change Fourth Assessment (IPCC AR4) twentieth-century simulations that have multiple realizations with a single model. The following six IPCC AR4 models all have at least four realizations of the twentieth-century simulations and are used in this study: the National Center for Atmospheric Research Community Climate System Model, version 3 (NCAR CCSM3) with eight, the Geophysical Fluid Dynamics Laboratory Climate Model version 2.1 (GFDL CM2.1) with five, the Goddard Institute for Space Studies Models E-H (GISS-EH) with five and E-R (GISS-ER) with nine, the Meteorological Research Institute Coupled General Circulation Model version 2.3.2a (MRI CGCM2.3.2a) with five, and the NCAR Parallel Climate Model (PCM) with four realizations.

Shown in Fig. 1 in colored lines are the NASSTI for the twentieth century from the six IPCC AR4 models with the known and estimated forcing of the greenhouse gas concentrations, aerosol, and natural solar and volcanic forcing prescribed. Each color line is the ensemble average of, variously, four to nine realizations of the twentieth century as simulated by each of the models. The trend of increasing SST over the North Atlantic basin in these models is similar to that observed (black line), but the amplitude of the oscillatory component is less than in observations. All of the models capture the rapid increase in temperature in the recent 2 decades. Because averaging over multiple realizations will tend to isolate the forced signal and suppress internally generated variations that are uncorrelated between realizations, this visual comparison suggests that observed, forced North Atlantic SST change was embedded within a large internal oscillation but that the recent warming was largely externally forced. However, the relatively small number of realizations in each of the model ensembles makes it difficult to draw a firm conclusion on the relative roles of internal and forced change in North Atlantic SST variations of the twentieth century.

One way to quantify the relative contribution of externally forced variability to total variability is the analysis of variance (ANOVA) method, which computes the ratio of the forced variance and the total variance. This method has been commonly used in separating the SST-forced variability from the total variability in prescribed SST experiments with multiple realizations (e.g., Harzallah and Sadourny 1995). In this study, we extend this method to estimate the internally and externally forced surface temperature variances in each of the coupled ocean–atmosphere models with prescribed anthropogenic, solar, and volcanic forcing.

If σ_I^2 and σ_a^2 represent the biased estimates of the internal and ensemble averaged variances, respectively, for the coupled ocean–atmosphere model, then

$$\sigma_I{}^2 = \frac{1}{MN}\sum_m\sum_n\left(\mathrm{Ts}_{mn} - \frac{1}{N}\sum_n \mathrm{Ts}_{mn}\right)^2$$

$$\sigma_a{}^2 = \frac{1}{M}\sum_m\left(\frac{1}{N}\sum_n \mathrm{Ts}_{mn} - \frac{1}{MN}\sum_m\sum_n \mathrm{Ts}_{mn}\right)^2,$$

where Ts_{mn} is the surface temperature for year m and ensemble member n, M is the total number of years, and N is the total number of ensemble members. The ratio of forced variance and total variance can be obtained as

$$r = \frac{\sigma_F{}^2}{\sigma_T{}^2} = \frac{\sigma_a{}^2 - \dfrac{1}{(N-1)}\sigma_I{}^2}{\sigma_T{}^2}, \quad \text{with}$$

$$\sigma_F{}^2 = \sigma_a{}^2 - \frac{1}{(N-1)}\sigma_I{}^2$$

$$\sigma_T{}^2 = \sigma_I{}^2 + \sigma_F{}^2.$$

The second term in the forced variance estimate ($\sigma_F{}^2$) removes the effect of internal variability contained in the ensemble average variance due to the small ensemble size. For a relatively large ensemble (say, $N > 20$), $\sigma_F{}^2$ should be well approximated by $\sigma_a{}^2$. In a relatively small ensemble and in the presence of large internal variability, $\sigma_F{}^2$ can be overcorrected and even result in negative value in some areas.

Figure 3 shows the variance ratio for decadal time scale variations averaged across the six models (variances are computed after subjecting the data to Butterworth filter). Most of the tropics (30°S–30°N) show that forced variance can account for 70% or more of the total variance. The largest ratio is found over Indian Ocean, indicating that decadal changes in the Indian Ocean SST are largely a response to external (radiative) forcing (Hurrel et al. 2004; Knutson et al. 1999). Over the eastern tropical Pacific, there is a local minimum in the forced variance ratio, suggesting that the model internal variability associated with tropical SST variability on decadal time scales is significant. In the extratropics and over land, forced variance accounts for as much as

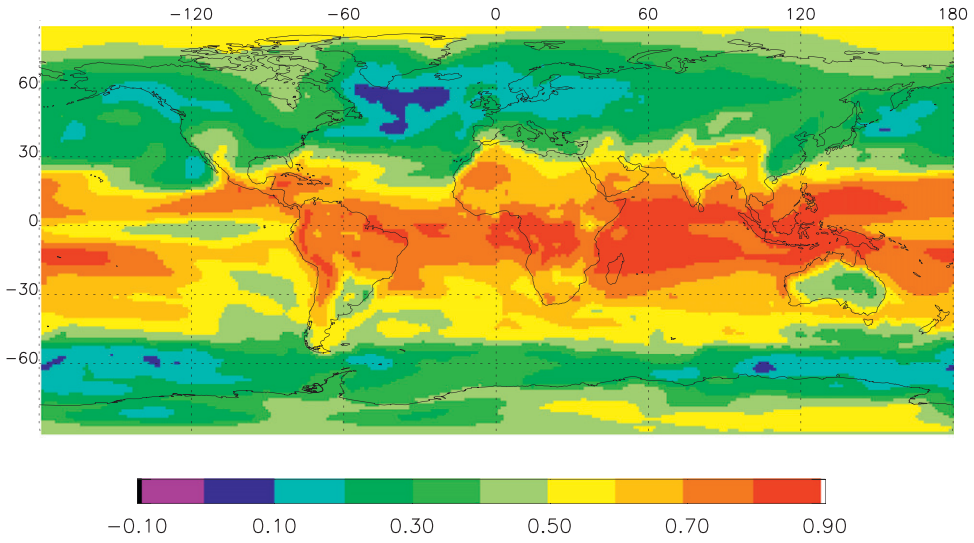

FIG. 3. Ratio of externally forced variance and the total variance averaged for the six IPCC AR4 coupled models with at least four ensemble members for the twentieth century. See details in the text.

50% of the total surface temperature variance. The lowest ratio is found over the extratropical North Atlantic, with ratio as low as 2%–10%, indicating the existence of strong internally forced decadal SST variations there. Small variance ratios are also found over other extratropical ocean regions, between 30° and 60°N in the Pacific, and in the Southern Ocean near 60°S. The variance ratios may not be well represented over the extratropical oceans because of the large internal variability there and the small number of ensemble members available. Figure 3 does, however, indicate clearly that internal variability is important over the extratropical oceans, in particular the North Atlantic, which is the subject of our investigation (note that the effect of the North Atlantic is felt into Europe as well).

To get the ratio of variance for the North Atlantic SST index, we repeated the same variance ratio calculation with the North Atlantic basin-averaged SST (averaged over the entire North Atlantic from 0° to 60°N). The ratio varies from 34% to 87% depending on the model, indicating that although external forcing is responsible for a large portion of spatially coherent, decadal surface temperature variations there, nonetheless internal variability is significant. For a North Pacific basin average, the variance ratio ranges from 70% to 91% depending on the model, whereas for the tropical SST between 30°S and 30°N, the numbers are above 93%. In the next section, a quantitative method will be used to extract the forced variability from the total and determine its spatial and temporal pattern and, as a residual, the dominant pattern of internal variability in the Atlantic Basin.

3. Forced and internal variability using signal-to-noise maximizing EOF analysis

A rigorous technique to define the forced variability, given multiple realizations of the coupled model simulations, is the signal-to-noise maximizing EOF analysis (Allen and Smith 1997; Venzke et al. 1999; Chang et al. 2000). The method applies a spatial prewhitening transformation to the model output, which removes the spatial correlations in the internal atmospheric variability (i.e., ''climate noise'') contained in the ensemble average. Thus, the spatial covariance in the ensemble average is purely due to the forced responses. Figure 4 shows the multimodel average of the spatial pattern (Fig. 4a) and the corresponding individual-model principal components (PCs) for the dominant mode (Fig. 4b) of the signal-to-noise (S/N) maximizing EOF analysis, using the six models listed above (section 2). This first EOF explains 55%–72% of the total model variance except the GISS-EH model, which only explains 37%. However, the second mode explains only 3%–6% in all models. This indicates that on decadal time scales, the externally forced variability can be represented rather decisively by a single, globally synchronous pattern. The spatial structure of the first mode is rather similar from model to model (not shown). Averaged over all models, it displays a largely global warming over both land and ocean areas. Note, however, that the pattern exhibits considerable spatial variation and even several patches of cooling over the North Atlantic, North Pacific, and in the Southern Hemisphere near 60°S. These variations are likely caused by such factors as local ocean dynamics and/or the uneven

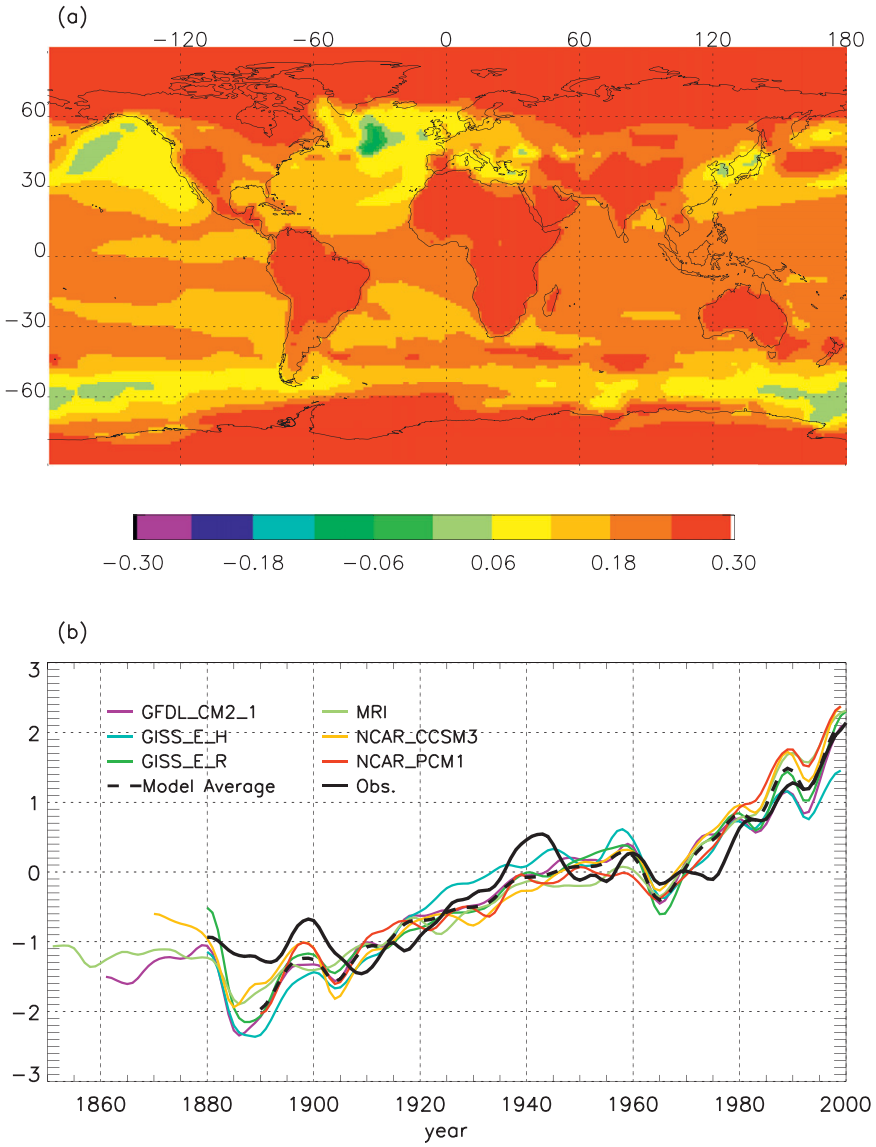

FIG. 4. (top) The multimodel mean spatial structure of the first mode of the S/N-maximizing EOF analysis averaged over the six IPCC AR4 models used in this study. Shown are regressions of annual-mean, low-pass-filtered surface temperature on the S/N-maximizing PC1. (bottom) S/N-maximizing PC1 for each of the six models. The colored lines are for the individual coupled ocean–atmosphere models; the dashed black line shows the six-model average PC1; the solid black line is the standardized global mean surface temperature from the GISS surface temperature dataset.

distribution of clouds and aerosol effects. In particular, a similar S/N-maximizing EOF analysis applied to model integrations with 1% year^{-1} CO_2 concentration increase but without any aerosol forcing (not shown) displays no negative centers over the North Pacific but does show a similar cooling over extratropical North Atlantic, indicating that the North Pacific cooling in Fig. 4a might be due to aerosol forcing, whereas the North Atlantic cooling is likely a result of the combined effect of aerosol forcing and internal ocean dynamics.

The first principal component (PC1) of each of the models (Fig. 4b) show a similar temporal trend with almost linear increases from the beginning of the twentieth century to 1960 and a small dip in the sixties followed by a sharper increase from the 1970s to the present. The black dashed line in Fig. 4b is the average PC for the six models and the solid black line is the standardized, global-mean observed surface temperature (air temperature over land and SST over the oceans). The similarity among the model PCs and between model

TABLE 1. Correlation coefficient between S/N-maximizing PC1 and ensemble average global mean surface temperature index (Tg), global mean sea surface temperature index (SSTg), global mean surface temperature over land (TLg), Indian Ocean SST index (IOSST), and the North Atlantic SST index (NASSTI) for each of the participating models and the observations.

	NCAR	GFDL	GISS-EH	GISS-ER	MRI	PCM	Model ensemble ranges	Observed
Tg	0.996	0.983	0.977	0.997	0.998	0.991	0.840–0.988	0.945
SSTg	0.998	0.987	0.981	0.994	0.997	0.986	0.921–0.988	0.926
TLg	0.996	0.982	0.962	0.991	0.993	0.973	0.816–0.988	0.897
IOSST	0.987	0.993	0.965	0.995	0.987	0.974	0.916–0.979	0.881
NASSTI	0.927	0.927	0.680	0.914	0.989	0.851	−0.07–0.959	0.658

and observations in Fig. 4b indicates that the method effectively isolates the global warming signal; although the global mean surface temperature is a good approximation for the observed forced signal, the AMO signature is discernable in the global mean surface temperature (e.g., the peak in the 40s and the dip in the 70s).

To quantify the extent to which the S/N-maximizing PC1 represents the ensemble mean variability of each model's surface temperature averaged over different regions of the globe, we computed its correlation coefficient with the following indices: global mean surface temperature, global mean SST, global mean surface temperature over land (TLg), North Atlantic SST, and Indian Ocean SST (IOSST) in Table 1. The Indian Ocean SST is included here because of the uniformly large forced variance ratio across all models in Fig. 3. Clearly, the S/N-maximizing PC1 is highly correlated with the global mean SST and global mean surface temperature in all models. The global mean land surface temperature and the Indian Ocean SST are slightly less well correlated with PC1 but still have correlations above 0.96 for all models. These high correlations are evidence of the global nature of the first EOF, as shown in Fig. 4a. Also shown in Table 1 are the correlations between PC1 and the North Atlantic SST. As expected (from Fig. 3), these correlations are lower than that with the other indices, consistent with the notion that there are large internally generated multidecadal variations in this region, and ensemble averaging with limited ensemble size cannot effectively remove all the internal variability. Two of the models (GISS-EH and NCAR PCM, which contain five and four ensemble members respectively) show particularly low correlations for the NASSTI index (0.68 and 0.85). It is interesting to compare the corresponding correlations for models that are close to these two in configurations—the GISS_ER (0.91) and NCAR CCSM (0.93), which have nine and eight ensemble members respectively—thus confirming the importance of large ensemble size in removing the internal variability.

The last column in Table 1 shows the correlation between the same SST indices as derived from observations and the model-averaged PC1. These correlations are expectedly lower than the corresponding ones for the models, likely because there is only one realization for the observations compared to at least four independent realizations for each of the IPCC models. It is also possible that the lower correlations are due to the inconsistency between forced change in the models and that in observations. The eighth column in Table 1 shows the range of correlation values between each of the indices discussed above and the models' PC1 using a single ensemble member instead of the ensemble mean. With the exception of Indian Ocean SST index, the correlations for observed SST indices (last column) are always within the range of values corresponding to a single model realization. The correlations between model-average PC1 and the observed SST indices decrease in the same way as in models, with the highest correlations obtained for global mean surface temperature and global mean SST. It illustrates that the separation of forced and natural North Atlantic SST using the global mean surface temperature and global mean SST, as shown in Fig. 2, is a good approximation for deriving the true forced variability. The observed North Atlantic SST index correlates much less well with PC1 compared to the other indices in Table 1, indicating a strong influence of internal variability there; this will be explored further below.

Next we projected each model's NASSTI onto the corresponding PC1 and defined that as the forced contribution to the secular change in the basin. A similar approach has been taken by Kravtsov and Spannagle (2008), who used multimodel average regional surface temperature as an indication for the externally forced signal. Figure 5a shows the forced trend of NASSTI so defined (color lines) along with the observed NASSTI (black line). Although there is a large spread for the forced NASSTI trends among the six models, it is clear that the observed NASSTI oscillates outside of the uncertainties of the model forced trend, consistent with the large internal component of the NASSTI in observations. One notices that the spread among the six models' forced NASSTI is larger at the beginning and

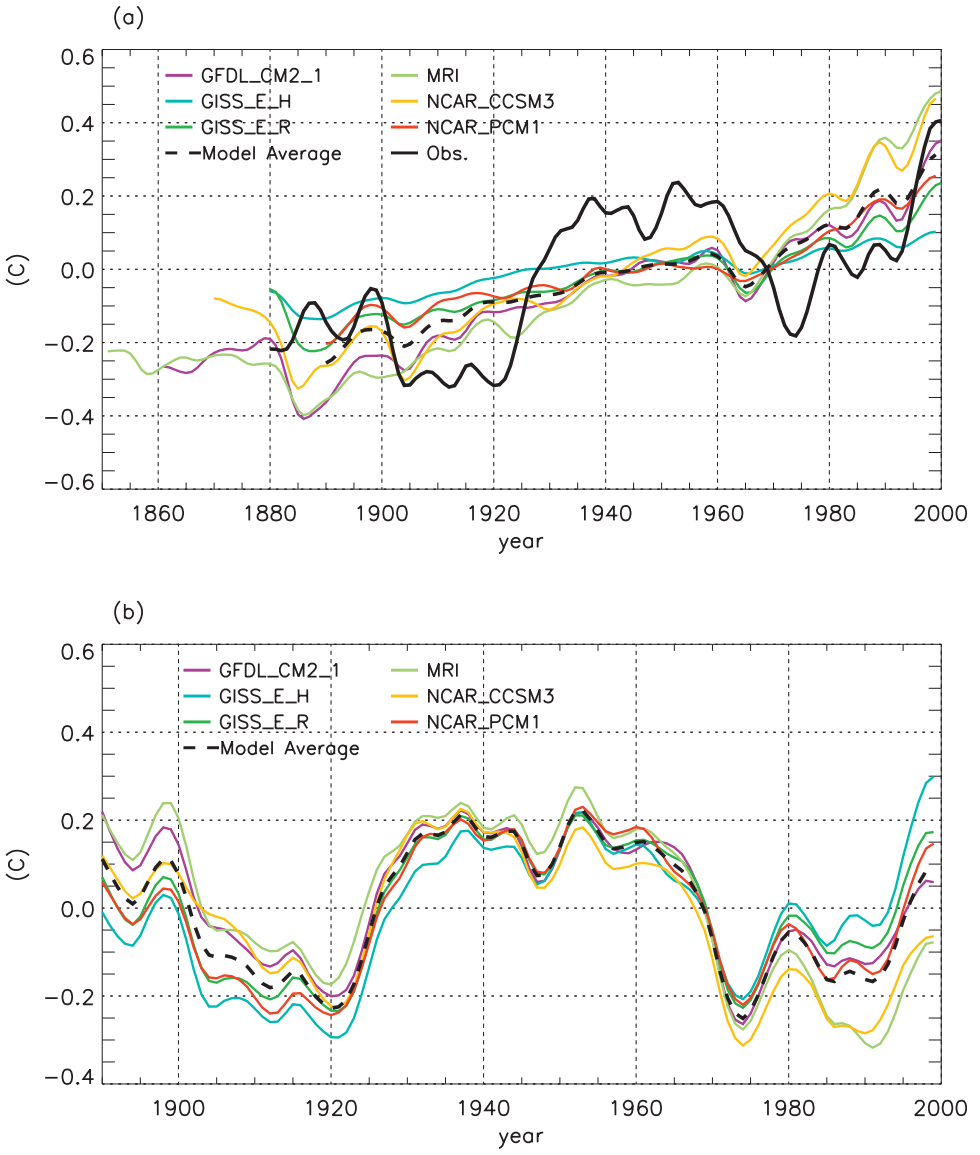

FIG. 5. (top) Projection of NASSTI onto the S/N-maximizing PC1 in each of the participating models (ensemble averaged, color lines) and observed counterpart (black line). (bottom) Observed internally generated AMO index constructed by subtracting from the observed index the model estimates of the forced NA SST shown in the top panel. The black dashed line in the bottom panel is the average across all six models.

the end of the twentieth century and much smaller in the middle of the century. This occurs because each model predicts a slightly different rate of North Atlantic SST increase. For example, the GISS-EH model has a much smaller rate of increase compared to that of MRI. Because the mean over the entire record was removed from each model's output, the plotted time series fan out at the ends. The Atlantic forced trends also show a larger spread among different models compared to that for the global mean SST and the Indian Ocean SST (not shown), but they are comparable to that for the North Pacific (not shown). The larger spread for the North Atlantic and North Pacific may reflect the uncertainties in model estimates of forced trends over the ocean basins where internal variability is large (Fig. 3). Given the uncertainties, we note that the observed temperature increases from the 1920s to the 1940s and during the most recent decade, as well as the cooling trend between 1960 and the mid-1970s, are larger than any of the forced trends in the models. Thus, Fig. 5a indicates clearly that the observed decadal variations in NASSTI cannot be explained by the response to external forcing

alone. An internal oscillatory component must be part of the North Atlantic SST variability.

To remove the model-based estimate of the forced change from the observed North Atlantic SST record, we averaged the six models' forced changes (the black dashed line in Fig. 5a) and subtracted it from the observed time series. The uncertainty in this estimate is represented by the spread generated when each model's forced component is separately removed from the data (see Fig. 5b). The amplitude of the oscillation, to which we hereafter refer to as AMO, is between −0.3° and +0.2°C, which is comparable to the detrended NASSTI in Fig. 2a but larger than those in Figs. 2c and 2e. In terms of the phase of the oscillation, Fig. 5b indicates that the AMO so defined is similar to that using the global mean surface temperature or global mean sea surface temperature as the forced signal (and shown in Fig. 2). In all of these definitions, the AMO crosses to the positive phase near the end of the twentieth century. Although the global averages pinpoint the inflections of the AMO well, they underestimate the amplitude by about 20%.

To relate the results to multidecadal Atlantic hurricane intensity variations, it is important to examine the twentieth-century tropical North Atlantic SST variations in the so-called hurricane main development regions (MDRs) as defined in earlier studies (Goldenberg and Shapiro 1996; Goldenberg et al. 2001; Emanuel 2005). Figure 3 indicates that the forced variance over the tropical North Atlantic accounts for a much larger portion of the total variance compared to the northern North Atlantic in all models. This is broadly consistent with Mann and Emanuel (2006), who argued that there is no internal oscillation in MDR SST variability after removing the forced signal due to both greenhouse warming and aerosol effect. The observed situation is depicted in Fig. 6a, which shows the projections of MDR-averaged SST for August–October (ASO) onto the S/N-maximizing PC1 for each model (colored lines), the model average (dashed black line), and the observations (solid black line). Figure 6a shows that the recent warming of the MDR is mainly due to external forcing and is similar in range to that of the North Atlantic basin-wide averages. Santer et al. (2006) analyzed the twentieth-century SST trend in the Atlantic and Pacific tropical cyclone regions and concluded that the twentieth-century trend cannot be explained by internal variability alone and that a larger share of the variability is explained by external forcing. Viewed over the entire century, our findings are consistent with their results. However, an examination of Fig. 6b, showing the difference between the observed MDR SST and the forced component as represented by the color lines in Fig. 6a, indicates that even in the MDR the contribution of internal variability is important. The latter is responsible for the sharp 1930s temperature rise and the 1970s temperature drop in the tropical North Atlantic, consistent with arguments made by, for example, Goldenberg et al. (2001). However, as far as the temperature rise in the last 2 decades or so is concerned, the contribution due to internal variability is not negligible, but it is not the dominant contributor. We stress that the MDR SST variability does not directly infer Atlantic hurricane activities and the number of landfalling hurricanes. Other factors such as vertical wind shear and static instability are known to play important roles in hurricane variability, which is not included in the discussion of this paper but may be associated with the Atlantic SST fluctuations (Wang et al. 2008).

4. Climate impacts of forced and natural North Atlantic SST variability

Recent studies (Enfield et al. 2001; McCabe et al. 2004; Sutton and Hodson 2005) have emphasized the impact of the AMO on North American and European precipitation. These studies defined the AMO as the low-pass, linearly detrended, North Atlantic–averaged SST anomaly. We have argued in this study that the AMO should be defined differently and that the resulting AMO phase changes then differ from the linearly detrended result. In the following, we contrast the climatic impacts of the externally forced North Atlantic SST trend and the AMO as defined in this study. To that end, we computed the regression between the observed global surface temperature and land precipitation with the forced NASSTI as defined by the multimodel average projection of the model's NASSTI onto S/N-maximizing PC1 (black dashed line in Fig. 5a) and the AMO (black line in Fig. 5b). A Monte Carlo statistical significance test[2] is applied to these regressions and only those with regression values significant at the 5% level are shown in Fig. 7.

Figure 7a is the externally forced ''global warming'' pattern for the twentieth century. By definition this is the same pattern that would emerge if the global field were regressed on the multimodel average of PC1. It is interesting to contrast this pattern with Fig. 4a, which displays the multimodel averaged depiction of the

[2] In the Monte Carle significance test here, the index time series is first randomized in temporal ordering and then applied the same recursive Butterworth filter before computing regression with precipitation and surface temperature. The regressions that are at or above the 97.5% or at or below the 2.5% level of all the randomized regressions were shown at the 5% statistical significance level.

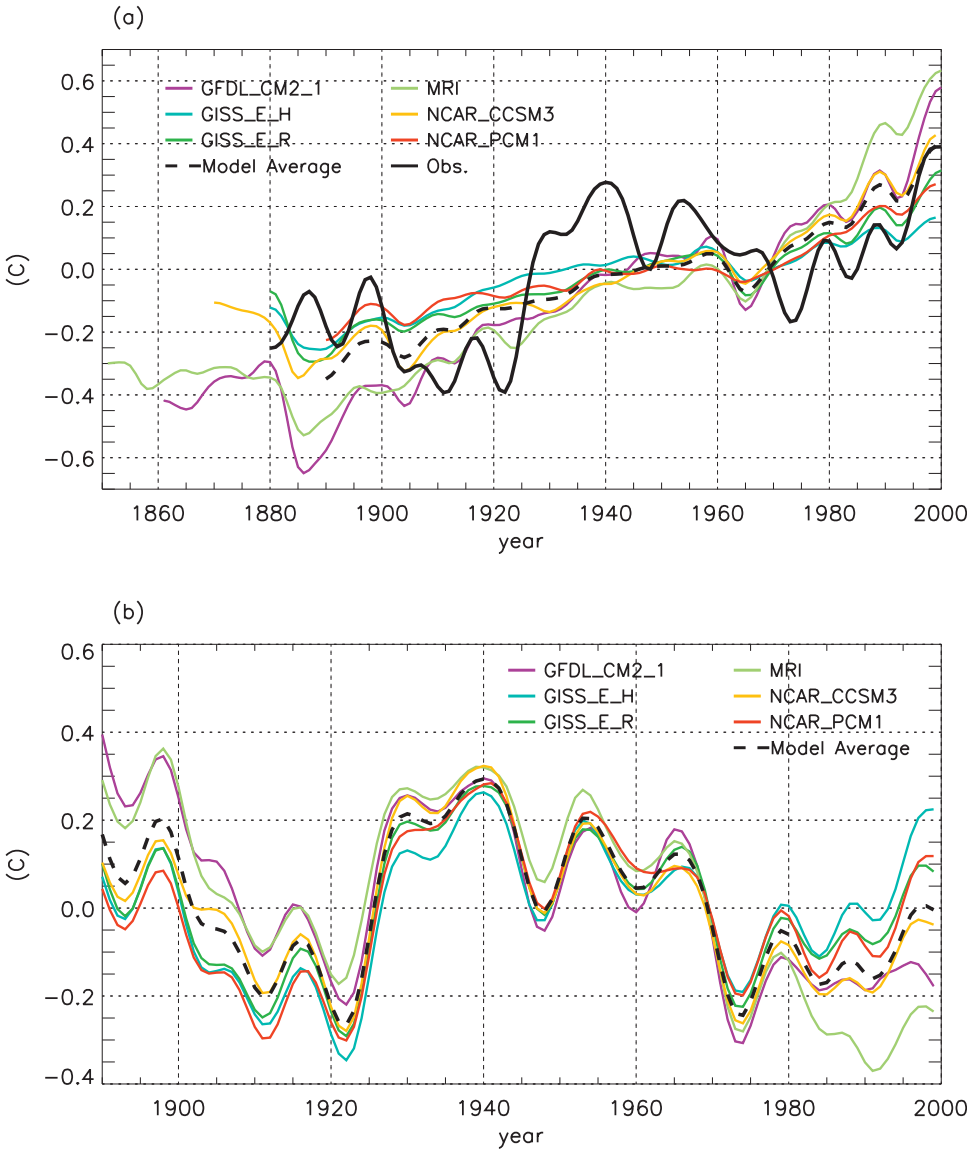

FIG. 6. Same as Fig. 5, but for MDR SST averaged over the 3-month hurricane season, August–October.

twentieth-century warming. As in the models, the observations displays a significant warming trend almost everywhere except the Southern Greenland coast in the North Atlantic, where a significant cooling occurred. However, the intensity of the observed warming over the tropical oceans is quite different from the simulated one. In particular, tropical Pacific Ocean SSTs have not warmed as much as in the model simulations. This may be due to the fact that there is considerable internal variation of tropical Pacific SSTs on decadal time scales and that the single observed "realization" of this variability masks the forced signal. It is also possible that response mechanisms not captured by the model reduce the impact of radiative forcing in this region (Cane et al. 1997). The influence of the tropical Pacific on the global climate is significant and hence it is important to investigate the ramification and causes of these differences, but this is beyond the scope of this paper.

For global land precipitation (Fig. 7c), however, the regression with the forced component is less significant than that for temperature. There are some indications of increased precipitation over northern high latitudes, but there is very little significant signal over the tropical and subtropical latitudes. A very slight hint of a drying trend over the western Sahel and the Mediterranean region can be noticed in Fig. 7c. Comparison with the same regression but using the coupled models' twentieth-century simulations (not shown) indicates a much stronger

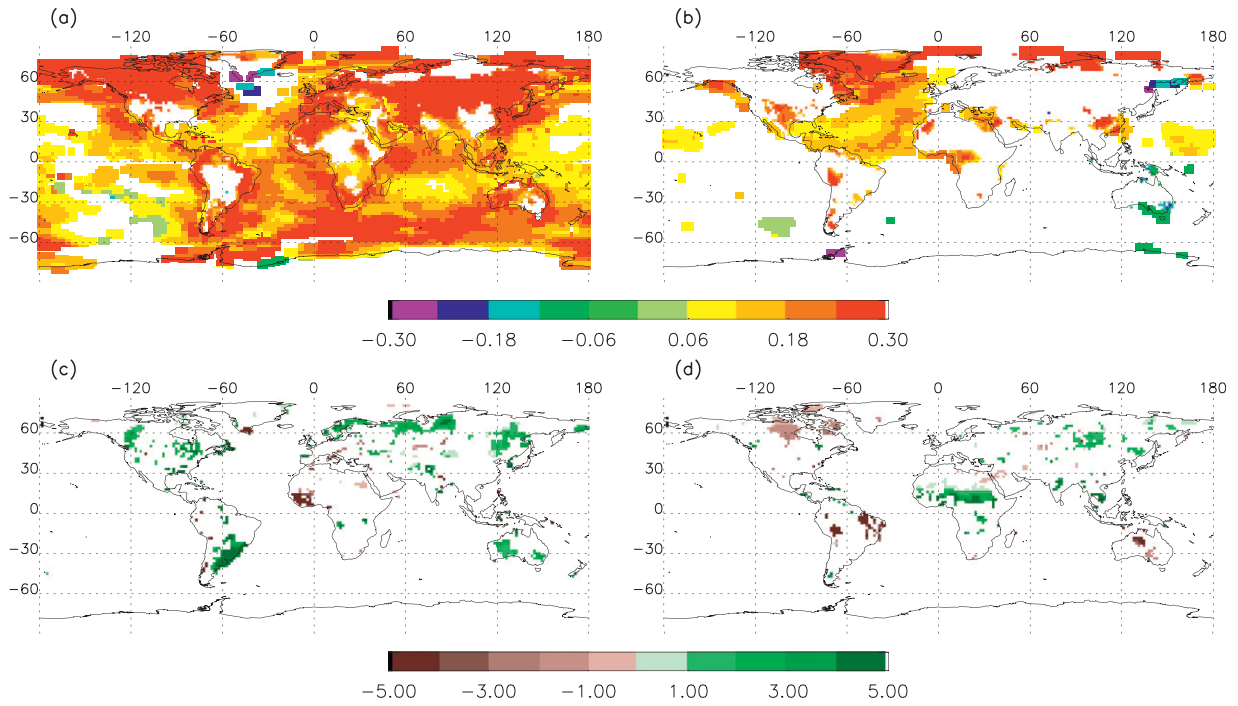

FIG. 7. Spatial pattern of regression between forced NA SST and the global surface (a) temperature and (c) precipitation, and between the naturally oscillating NA SST (AMO) and the global surface (b) temperature and (d) precipitation for the twentieth century. The land surface temperature and precipitation data are taken from CRU's 0.5° × 0.5° version and the SST over ocean is taken from GISS. Only the regression values that exceed the 5% statistical significance level based on Monte Carlo method (details in text) is plotted. Units are degrees Celsius per standard deviation of SST index for surface temperature and millimeters per month per standard deviation of SST index for precipitation.

subtropical drying, including Southern Mexico, the Caribbean, the Mediterranean, and the Sahel region (see Solomon et al. 2007). This apparent difference between the model and observations may be explained by the stronger tropical warming in coupled models, particularly in the Pacific, as discussed above. As shown in previous studies (e.g., Yin 2005), one of the robust responses of the atmospheric circulation to greenhouse forcing is northward-shifted storm tracks, which enhance precipitation in the high latitudes and drying in the subtropics (see also Held and Soden 2006). Figure 7 suggests that this mechanism may not be as advanced in reality as predicted in the coupled models, perhaps because of the lesser warming of the Pacific Ocean in observations compared to the model simulations. Further analysis is needed to confirm such connections.

The internally generated, AMO-related patterns in temperature and precipitation are generally consistent with the findings of previous studies. The temperature pattern (Fig. 7b) is characterized by basinwide warming over the North Atlantic and its surrounding regions. For precipitation (Fig. 7d), the most dominant feature is the positive anomaly over the Sahel associated with the warming phase of the AMO (Knight et al. 2006; Zhang and Delworth 2006), opposite to that associated with the externally forced warming. This is not surprising considering that the Atlantic SST patterns associated with external forcing (Fig. 7a) and the AMO (Fig. 7b) imply different polarities of the Atlantic interhemispheric SST gradient in the warm phase of the AMO and during global warming. The interhemispheric gradient is a key factor in determining the seasonal position of the Atlantic intertropical convergence zone (ITCZ), which governs rainfall over tropical Africa. Thus, when a global warming trend occurs with a cooling trend of the AMO, one would expect the Sahel to experience extreme drying conditions, such as was the case in 1960–70. Other features of the AMO-related precipitation anomalies are less significant, indicating drying of parts of North and South America and Australia and an enhanced Indian monsoon and rainfall over northern Asia.

Another interesting finding in Fig. 7 is the opposite impact of a warm AMO and the externally forced warming trend on South Greenland temperature. Although the externally forced trend is negative along the South Greenland coast, the AMO warming trend there is positive. This is consistent with the simulation of models examined in this study (not shown). A recent study

(Chylek et al. 2006) found that the warming of coastal Greenland during 1920–30 is much stronger than the recent warming trend, consistent with Fig. 7. Specifically, in 1920–30, the externally forced trend was weak and the AMO trend dominated. One should be aware that the temperature trend over central Greenland where the ice sheet lies is positive in both the forced and the internal component; thus, both contribute to a positive trend of surface temperature there in the recent decade. The recent rapid decrease in Greenland ice sheet volume (Serreze and Francis 2006) may be due to the additive effect of the forced warming trend and the transition to a positive phase in the internal component of the AMO. Given the short observational records, there may be overfitting in the regression analysis. Similar analysis based on model simulations is needed to confirm the observational relationship.

5. Summary

Using six of the IPCC AR4 twentieth-century simulations with multiple ensemble members, we are able to effectively separate the externally forced component of North Atlantic Ocean SST variations and the internally varying component using signal-to-noise (S/N)-maximizing EOF analysis. We further show that the observed North Atlantic SST variability is well outside of the uncertainty of the model-simulated forced trend, indicating the existence of an internal component in observations. The S/N-maximizing PC1 is found to be highly correlated with the ensemble mean and globally averaged SST and surface air temperature, indicating that these indices can be used, alternatively, to represent forced variations in the models and in observations.

Taking the model-averaged S/N PC1 as the forced North Atlantic SST trend, we found that the internal variability of North Atlantic SST, or the AMO, was at an upswing tendency at the end of the twentieth century and thus in phase with the forced tendency. If the AMO trend continues in this direction, the North Atlantic will experience much faster warming in the coming years than the rest of the world. It is further shown that the hurricane main development region SSTs for August, September, and October show a dominance of external forcing in the recent warming trend. However, the earlier warming trend in the 1930s and the cooling trend in the 1970s were connected mainly to internal variability.

The spatial pattern of surface temperature and precipitation associated with the externally forced trend and the AMO are examined using regression analysis. The observed externally forced anomalies show a global warming trend everywhere except the northern North Atlantic. However, this pattern differs from the modeled pattern in its details, particularly over the tropical Pacific. There are indications in the model simulations that the cooling trend over the northern North Pacific may be related to aerosol forcing. Because most of the IPCC AR4 model projections show a 25% slowing of the Atlantic meridional overturning circulation over the twenty-first century (Solomon et al. 2007), the strong cooling over the North Atlantic may be a result of the slowdown of ocean circulation. Consistent with previous observational studies on the impact of the AMO on precipitation around the Atlantic basin, we find that the largest impact is over the Sahel region, where the warming trend of the AMO is associated with increased precipitation. The Sahel drought of the 1970s and 1980s is associated with a cooling trend in the AMO. There are also indications of drought conditions associated with a warming trend in the AMO over South America and Australia.

The results presented here do not lead to dramatically different conclusions from the earlier studies dealing with the same issue. We believe, however, that our rigorous statistical analysis puts the claim that the North Atlantic displayed in the twentieth century an internal ''oscillation'' of considerable magnitude (compared to overall externally forced trend) on a more robust footing. We were also able to show that this internal variation led to sharp decadal changes in temperature, but due to its oscillatory nature these transitions led to an overall compensation on a century time scale. Moreover, we also argue that the globally averaged surface temperature appears to be a good proxy for the temporal march of externally forced variability and that most of the latter is globally synchronous, albeit nonuniform spatially. The smoothed, local expression of externally forced variability can therefore be represented by the regression of local variables such as temperature and precipitation on the smoothed time series of global mean surface temperature. This expression should obviously be quantified by an error estimate based on standard approaches to error analysis, either parametric or nonparametric.

Our results point at the importance of internal variability, specifically the AMO, in determining future changes in climate. The AMO may continue its upward trend and contribute to positive North Atlantic SST anomalies in the near future, given its past temporal evolution and the fact that it crosses to the positive phase at the end of the twentieth century. Assuming a linear superposition of the forced and natural responses, the North Atlantic may experience unprecedented warming in the next decade or so when combined with a strong externally forced, anthropogenic global warming trend. However, if the AMO trend is reversed in the coming years (N. Keenlyside et al. 2008, personal communication),

the warming of most of the North Atlantic will lag other regions and this will similarly influence northeastern North America, western Europe, and the Mediterranean. The accurate prediction of the AMO phase transition is thus important for the future, near-term climate change prediction. Determining the nature and realism of the AMO in coupled ocean–atmosphere models is an important next step leading to a better understanding of the AMO dynamics and its predictability.

Acknowledgments. We thank Dr. Isaac Held for many useful discussions and suggestions for this work. Thanks are also due to Drs. Michela Biasutti, Mark Cane, Tom Delworth, Alessandra Giannini, and Lisa Goddard for helpful discussions and to two anonymous reviewers for their many constructive comments. The work was supported by NOAA Grant NA030AR4320179 on abrupt climate change.

REFERENCES

Allen, M. R., and L. A. Smith, 1997: Optimal filtering in singular spectrum analysis. *Phys. Lett.,* **234,** 419–428.

Cane, M. A., A. C. Clement, A. Kaplan, Y. Kushnir, D. Pozdnyakov, R. Seager, S. E. Zebiak, and R. Murtugudde, 1997: Twentieth-century sea surface temperature trends. *Science,* **275,** 957–960.

Chang, P., R. Saravanan, L. Ji, and G. C. Hegerl, 2000: The effect of local sea surface temperatures on atmospheric circulation over the tropical Atlantic sector. *J. Climate,* **13,** 2195–2216.

Chylek, P., M. K. Dubey, and G. Lesins, 2006: Greenland warming of 1920–1930 and 1995–2005. *Geophys. Res. Lett.,* **33,** L11707, doi:10.1029/2006GL026510.

Emanuel, K. A., 2005: Increasing destructiveness of tropical cyclones over the past 30 years. *Nature,* **436,** 686–688.

Enfield, D. B., A. M. Mestas-Nuñez, and P. J. Trimble, 2001: The Atlantic multidecadal oscillation and its relation to rainfall and river flows in the continental U.S. *Geophys. Res. Lett.,* **28,** 2077–2080.

Goldenberg, S. B., and L. J. Shapiro, 1996: Physical mechanisms for the association of El Niño and West African rainfall with Atlantic major hurricane activity. *J. Climate,* **9,** 1169–1187.

——, C. Landsea, A. M. Mestas-Nuñez, and W. M. Gray, 2001: The recent increase in Atlantic hurricane activity: Causes and implications. *Science,* **293,** 474–479.

Harzallah, A., and R. Sadourny, 1995: Internal versus SST-forced atmospheric variability as simulated by an atmospheric general circulation model. *J. Climate,* **8,** 474–495.

Held, I. M., and B. Soden, 2006: Robust responses of the hydrological cycle to global warming. *J. Climate,* **19,** 5686–5699.

Hurrel, J. W., M. P. Hoerling, A. S. Phillips, and T. Xu, 2004: Twentieth century North Atlantic climate change. Part I: Assessing determinism. *Climate Dyn.,* **23,** 371–389.

Kerr, R. A., 2000: A North Atlantic climate pacemaker for the centuries. *Science,* **288,** 1984–1986.

Knight, J. R., C. K. Folland, and A. A. Scaife, 2006: Climate impacts of the Atlantic Multidecadal Oscillation. *Geophys. Res. Lett.,* **33,** L17706, doi:10.1029/2006GL026242.

Knutson, T. R., T. L. Delworth, K. W. Dixon, and R. J. Stouffer, 1999: Model assessment of regional surface temperature trends (1949–1997). *J. Geophys. Res.,* **104,** 30 981–30 996.

Kravtsov, S., and C. Spannagle, 2008: Multidecadal climate variability in observed and modeled surface temperatures. *J. Climate,* **21,** 1104–1121.

Kushnir, Y., 1994: Interdecadal variations in North Atlantic sea surface temperature and associated atmospheric conditions. *J. Climate,* **7,** 141–157.

Landsea, C. W., 2005: Hurricanes and global warming. *Nature,* **438,** E11–E12, doi:10.1038/nature04477.

Mann, M. E., and K. Emanuel, 2006: Atlantic hurricane trends linked to climate change. *Eos, Trans. Amer. Geophys. Union,* **87,** 233–244.

McCabe, G. J., M. A. Palecki, and J. L. Betancourt, 2004: Pacific and Atlantic Ocean influences on multi-decadal drought frequency in the United States. *Proc. Natl. Acad. Sci. USA,* **101,** 4136–4141, doi:10.1073/pnas.0306738101.

Santer, B. D., and Coauthors, 2006: Forced and unforced ocean temperature changes in Atlantic and Pacific tropical cyclogenesis regions. *Proc. Natl. Acad. Sci. USA,* **103,** 13 905–13 910.

Schlesinger, M. E., and N. Ramankutty, 1994: An oscillation in the global climate system of period 65–70 years. *Nature,* **367,** 723–726.

Serreze, M. C., and J. A. Francis, 2006: The Arctic on the fast track of change. *Weather,* **61,** 65–69.

Solomon, S., D. Qin, M. Manning, M. Marquis, K. Averyt, M. M. B. Tignor, H. L. Miller Jr., and Z. Chen, Eds., 2007: *Climate Change 2007: The Physical Science Basis*. Cambridge University Press, 996 pp.

Sutton, R. T., and D. L. R. Hodson, 2005: Atlantic Ocean forcing of North American and European summer climate. *Science,* **309,** 115–118.

Trenberth, K. E., and D. J. Shea, 2006: Atlantic hurricanes and natural variability in 2005. *Geophys. Res. Lett.,* **33,** L12704, doi:10.1029/2006GL026894.

Venzke, S., M. R. Allen, R. T. Sutton, and D. P. Rowell, 1999: The atmospheric response over the North Atlantic to decadal changes in sea surface temperature. *J. Climate,* **12,** 2562–2584.

Wang, C., S.-K. Lee, and D. B. Enfield, 2008: Climate response to anomalously large and small Atlantic warm pools during the summer. *J. Climate,* **21,** 2437–2450.

Webster, P. J., G. J. Holland, J. A. Curry, and H.-R. Chang, 2005: Changes in tropical cyclone number, duration, and intensity in a warming environment. *Science,* **309,** 1844–1846.

Yin, J. H., 2005: A consistent poleward shift of the storm tracks in simulations of 21st century climate. *Geophys. Res. Lett.,* **32,** L18701, doi:10.1029/2005GL023684.

Zhang, R., and T. Delworth, 2006: Impact of Atlantic multidecadal oscillations on India/Sahel rainfall and Atlantic hurricanes. *Geophys. Res. Lett.,* **33,** L17712, doi:10.1029/2006GL026267.